# Wide-range wavelength and angle resolved light scattering measurement setup

Marin Fouchier, Myriam Zerrad, Michel Lequime, Claude Amra

Optics Letters

# Wide-range wavelength and angle resolved light scattering measurement setup

Marin Fouchier,[1,2] Myriam Zerrad,[1] Michel Lequime,[1,*] and Claude Amra[1]

[1]Aix Marseille Université, CNRS, Centrale Marseille, Institut Fresnel, Marseille, France
[2]Centre National d'Etudes Spatiales, Toulouse, France
*Corresponding author: michel.lequime@fresnel.fr

Received 3 March 2020; revised 27 March 2020; accepted 30 March 2020; posted 31 March 2020 (Doc. ID 392000); published 21 April 2020

**We present a new version of a light scattering measurement setup, using a high-power supercontinuum laser source, two volume hologram filters, and two low-noise scientific grade cameras. This configuration enables spectral and angle resolved characterization of the light scattered by complex thin-film filters from 400 to 1650 nm. Measurements carried out on specific filters illustrate the performances of the setup.** 

https://doi.org/10.1364/OL.392000



The improvements achieved over the last three decades in both optical filter design software and thin-film coatings deposition processes have enabled the production of interference filters with levels of performance commensurate with various demanding areas of application, such as light detection and ranging [1,2], fluorescence microscopy [3], fiber-optic telecommunications [4], or space instruments [5,6]. The functions of these multilayer stacks are mainly band-pass, edge, or notch filtering, characterized by a high level of transmittance in their pass-band (>95%), sharp spectral edges (>40 dB/nm), and a high level of rejection in their stop-band, with optical densities (ODs) often greater than eight.

In addition to these spectral transmittance and reflectance properties, the level of scattering introduced by these filters is also a key performance parameter, especially for imaging applications such as Earth observation from space. Indeed, light scattering critically affects the performance of such an instrument by altering image quality and generating cross-talk between separate spectral bands. Therefore, an accurate measurement of the scattering properties of optical thin films over a wide range of wavelengths corresponding to the bandwidth of a multi-spectral imager is required to assess its performance at system level.

Numerous dedicated setups have been developed to perform such light scattering measurements [7–11], but most use powerful laser lines to attain the required sensitivity (typically $10^{-8}$ $sr^{-1}$) at one or more discrete wavelengths in the ultraviolet (325 nm), visible (405 nm, 532 nm, 633 nm), or near infrared (1064 nm, 1550 nm), which does not cover the whole spectral range but only discrete wavelengths.

Therefore, our objective was to develop an instrument that could record the bidirectional scattering distribution function (BSDF) of a multilayer component at any wavelength between 400 and 1650 nm with a spectral resolution around 1 nm and an angular resolution better than 1°. This new setup is an upgraded version of SALSA, a spectrophotometric instrument previously developed by our team [12,13] for ultra-fine characterization of the spectral transmittance of thin-film optical filters between 400 and 1000 nm and whose ultimate sensitivity corresponds to ODs close to 13.

Figure 1 shows a functional representation of this measurement setup; the parts added to the previous version are shown in blue.

First of all, the power of the supercontinuum laser source used in our previous setup [13] has been increased from 6 to 8 W by replacing the NKT Photonics EXB-6 with a FIANIUM WL-SC-400-8 [14]. A dichroic beam splitter (reference NKT Photonics Splitter-950-01) has been added to split the broadband spectrum delivered by this supercontinuum laser source (400 nm to 2.4 μm) into two channels: a visible channel (from 400 to 975 nm, shown in green) and an infrared channel (from 975 to 2400 nm, shown in red).

The optical items used in the visible channel are the same as those presented in our previous papers [12,13], namely, a tunable volume hologram filter from PHOTON Etc. [15], reference LLTF Contrast VIS HP8, covering the spectral range from 350 to 1100 nm (filter bandwidth around 2 nm), an electro-mechanical shutter (SH1), an order sorting device (OSD) used to clean the spectral profile of the filtered beam, a set of three remotely operated ODs (OD1), and a fiber receiving assembly consisting of a parabolic off-axis reflective collimator (ORC, focal length $f = 15$ mm) associated with a multimode fiber-optic link (FOL1, core diameter $2a = 50$ μm). Moreover, a non-polarizing beam splitter (BS1) reflects a small portion (a few %) of the incoming visible beam toward a reference arm that incorporates a reflective collimator (RC R1, focal length 15 mm), a multimode optical fiber (FOL R1, core diameter 50 μm), and a silicon photoreceiver (VIS PD) from FEMTO [16], reference DE-OE-200-Si.

The structure of the infrared channel is similar to that of the visible channel, and thus includes a volume hologram filter from PHOTON Etc. [15], reference LLTF Contrast SWIR HP8

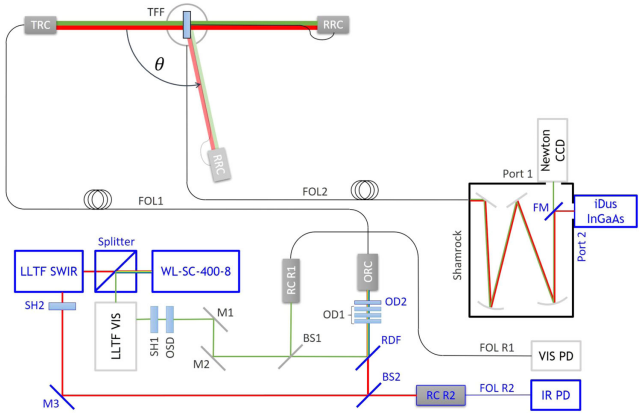


**Fig. 1.** Spectral and angular light scattering characterization apparatus. WL-SC-400-8, supercontinuum laser; LLTF VIS and LLTF SWIR, tunable volume hologram filters; SH, shutter; OSD, order sorting device; RDF, recombination dichroic filter; Shamrock, Czerny–Turner monochromator; Newton charge-coupled device (CCD), scientific grade CCD camera; iDus InGaAs, scientific grade InGaAs camera; VIS PD, Si photodiode; IR PD, InGaAs photodiode.

(wavelength range 800 to 2300 nm, spectral bandwidth around 3.5 nm), an electro-mechanical shutter (SH2), a beam splitter (BS2), and a reference arm dedicated to this infrared channel and consisting of a reflective collimator (RC R2), an optical fiber (FOL R2), and an InGaAs photoreceiver (IR PD) from FEMTO [16], reference DE-OE-200-In1.

A dichroic filter (RDF) from IRIDIAN Spectral Technologies [17] is used to recombine the infrared and visible beams, their fine alignment being achieved by adjusting the spatial and angular positions of both M3 and BS2 reflective elements. This fine alignment ensures the perfect coupling of both beams into the fiber-optic link FOL1. An extra OD (OD2) is inserted in the recombined beam, before the reflective collimator ORC, to increase the level of attenuation for the infrared channel. The total OD seen by the main beam (visible or infrared) can thereby be adjusted between zero and 10 in steps close to one (this value is wavelength dependent but known by calibration).

By connecting the end of the fiber-optic link FOL1 to the focal plane of a reflective collimator (TRC), we can illuminate the thin-film filter sample (TFF) with a low divergence beam (approximately 0.1°) whose central wavelength can be selected continuously between 400 and 1650 nm. This central wavelength is defined by opening one of the shutters (SH1 or SH2) and tuning the corresponding volume hologram filter (LLTF VIS or LLTF SWIR). The diameter of the beam at the surface of the sample is around 6 mm. The light scattered by the sample in the direction defined by $\theta$ (see Fig. 1) is collected by a fiber collimator consisting of an off-axis parabolic mirror (RRC, focal length 15 mm) whose focal plane is fitted with a multimode fiber optic (FOL2, core diameter 105 μm).

The extremity of this optical fiber is connected to the entrance port of a Czerny–Turner monochromator from ANDOR [18], reference Shamrock SR-193i-B1. Two gratings are mounted back-to-back on the motorized turret of this spectrometer. The first is an 1800-lines-per-millimeter holographic grating, optimized for the spectral range from 360 to 1100 nm, while the second is a ruled grating with 760 lines per millimeter and optimized for the spectral range between 850 nm and 2 μm. The two output ports of this spectrometer are fitted with low-noise scientific grade cameras, namely, a backlit, visible-optimized anti-fringing CCD camera from ANDOR [18], reference NEWTON DU920P-BVF, on the direct output port 1 (255 × 1024 pixels of 26 × 26 μm each) and an iDus InGaAs 1.7 μm linear array detector, again from ANDOR [18], reference DU491A, on the side output port 2 (1024 pixels of 25 × 500 μm each). A silver-coated flip mirror (FM) is used to select one of these two output ports in accordance with the central wavelength chosen for the illuminating beam.

The measurement procedure is similar to the one described in our previous papers [12,13]. To measure the amount of light scattered by a filter at an angle $\theta$ and a wavelength $\lambda$, for instance, 60° and 1150 nm, the sequence is as follows: rotate the measurement arm to the chosen angle $\theta$, close the shutter SH1, tune the SWIR LLTF to the selected wavelength $\lambda$, rotate the motorized turret of the Shamrock monochromator to the position that corresponds to this wavelength for the ruled grating for the SWIR range, and flip the output port mirror to the side position. The apparatus is then ready to make the first measurement at this specific wavelength; this starts by defining a set of ODs (OD1, OD2), an opening duration $\tau$ for the shutter SH2, and an integration time for the iDus camera, slightly greater than $\tau$. The two free parameters (opening duration $\tau$, overall OD OD1 + OD2 inserted on the main beam) are simultaneously adjusted with the help of an optimized algorithm to ensure that the maximum level detected by the pixels of the InGaAs linear photodiode array is less than 70% of its saturation level. The video line provided by the camera is then recorded along with the 16-bit digitized signal provided by the IR PD channel over the integration time (sample rate 200 ksamples/s). Finally, the shutter SH2 is closed, and a new video line is recorded with the same integration time to determine the noise contribution to the signal. This last step is used only for the infrared channel, because the determination of this noise contribution can be achieved for the visible channel by using some specific lines of the CCD at the top and the bottom of the matrix that are not illuminated by the spatially dispersed beam: indeed, the height of the fiber image at the CCD level is about 110 μm (transverse magnification of the spectrometer $\gamma = 1.07$), in contrast with that of the CCD matrix, i.e., 255 × 26 = 6630 μm.

The use of a dispersive receiver at the end of the detection chain allows us, first, to improve the spectral resolution of the apparatus (approximately up to 0.25 nm for the visible channel and 0.6 nm for the infrared channel), and second to reduce the contribution of parasitic light. Moreover, the processing of the video line provided by each camera can be automatically adapted to the effective signal-to-noise ratio of the measurement.

We will now focus our experimental tests on the infrared channel of the setup, since the visible channel has already been characterized and qualified [19,20]. First of all, Fig. 2 illustrates its angular selectivity, showing a rejection level better than OD8 at 1° from the transmitted specular beam. This selectivity can be further improved by decreasing the core diameter of the FOL2 fiber optic link (e.g., 50 μm instead of 105 μm).

The absolute calibration of our scatterometer is achieved using a Spectralon white diffuse reflectance sample from LABSPHERE [21]. The angular variation of the signal, recorded, for instance, at $\lambda = 1115$ nm, is shown in Fig. 3 in comparison with the theoretical angle resolved scattering (ARS, in $sr^{-1}$) defined at the same wavelength by

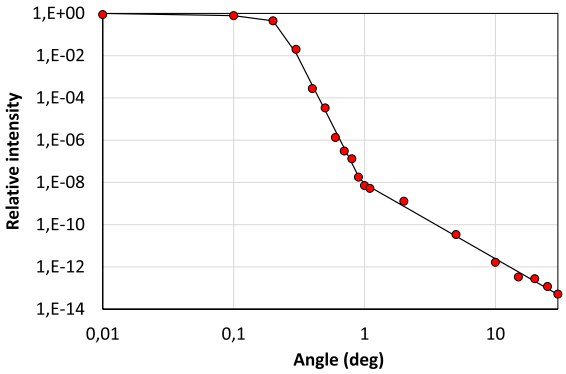


**Fig. 2.** Angular response of the setup to the direction defined by the transmitted specular beam (log–log units).

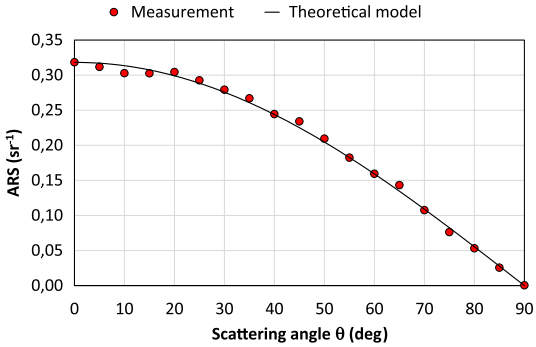


**Fig. 3.** Comparison between the theoretical ARS cosine model and the angular dependence of the signal measured on a Spectralon sample ($\lambda = 1115$ nm).

$$\mathrm{ARS}(\theta, \lambda) = \frac{1}{\pi}\rho(\lambda)\cos\theta, \tag{1}$$

where $\rho(\lambda)$ is the diffuse reflection coefficient of Spectralon at wavelength $\lambda$ ($\rho = 0.9832$ at $\lambda = 1115$ nm). The agreement is very satisfactory (note that the result of these calibration measurements is shown with a linear scale).

This demonstrates that our instrument is able to measure high levels of scattered light with great accuracy. To assess its ability to detect very low scattered levels, we also recorded the instrument signature, i.e., the angle resolved signal in the absence of a sample: at, e.g., $\lambda = 1115$ nm, this floor level is less than $10^{-8}$ sr$^{-1}$ in the whole angle range between 5° and 175°.

To validate the instrument's performance over the wavelength range from 900 to 1650 nm, we measured the spectral transmittance of four silver layers, of different thicknesses, deposited on silica substrates. We had conducted the same test on the visible range with the previous version of our setup [13], and the use of silver optical constants published by Johnson and Christy [22] allowed us to determine the thickness of each of these four layers, i.e., 23, 60, 124, and 256 nm. By using the same thickness values and the spectral dependence of silver constants in the wavelength range corresponding to the infrared channel, we can compare these extrapolated data with our new measurement results (see Fig. 4). The quality of concordance is excellent (standard deviation ≈ OD.04).

The last step of this validation procedure consists of verifying whether the spectral resolution of the infrared channel

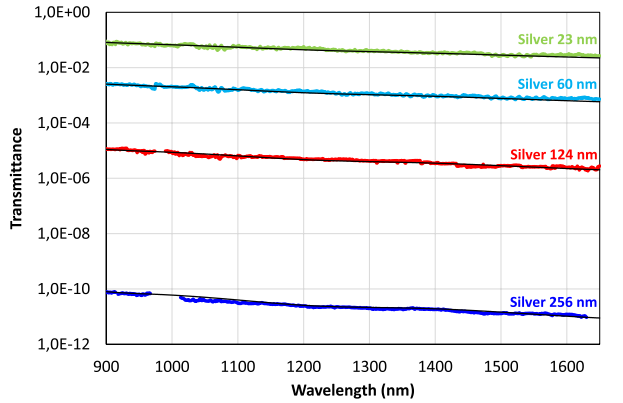


**Fig. 4.** Spectral transmittance of four silver layers measured with our setup (in green, thickness 23 nm; in light blue, thickness 60 nm; in red, thickness 124 nm; in dark blue, thickness 256 nm; black lines, extrapolated data using Johnson tables [22]).

meets our expectations. To this end, we measured the spectral transmittance of a band-pass test filter, centered at 1273 nm, incorporating around 100 alternating layers of $Nb_2O_5$ and $SiO_2$ deposited on a silica substrate (rear face uncoated). This was manufactured by the French company CILAS Ariane Group using a dual ion beam sputtering machine. The comparison between the design data and the measurement results derived from our setup is shown Fig. 5. Again, the agreement is nearly perfect, and the width of the narrow side peaks recorded around 1100 and 1500 nm at the edges of the filter's rejection band agrees very well with that defined by the design. Note that the transmission noise floor is less than $10^{-12}$ over most of the infrared channel spectral range.

Now we demonstrate the ability of this bench to measure the scattering properties of a complex interference filter in the infrared part of the spectrum. Figure 6 shows a false color representation of the spectral and angular dependences of the scattering level ARS ($\theta$, $\lambda$) of our test filter on the left calculated using a theoretical model [23] and on the right measured with the upgraded version of our setup. In both cases, the angle of incidence is 5°, the light is unpolarized, and the data steps are 5° and 5 nm. The left part of each graph corresponds to the reflected half-space (between 10° and 85°) and the right part

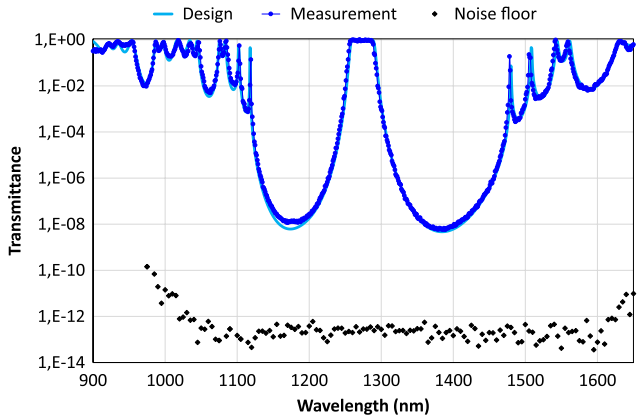


**Fig. 5.** Spectral transmittance of the test filter for an angle of incidence of 5° (design data, continuous light blue line; measurement, dark blue dots; noise floor, black diamonds).

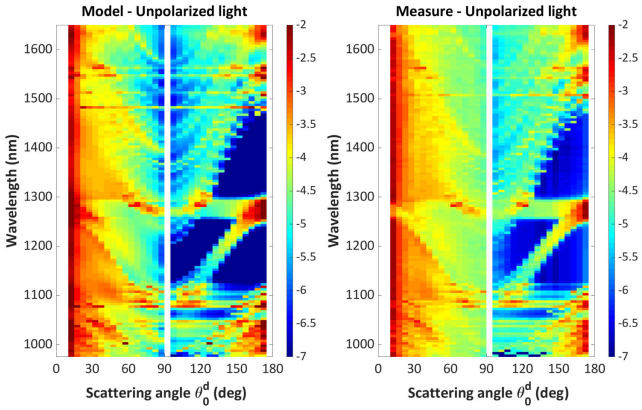


**Fig. 6.** False color representation of the angle and wavelength resolved scattering of test filter using a log scale (on the left, theoretical modeling; on the right, experimental measurement).

to the transmitted half-space (between 95° and 170°). The color map is identical for both graphs (log scale). Taking into account the complexity of this test filter (around 100 layers), the agreement is remarkable: indeed, all the spectral and angular patterns predicted by our model, in both location and level, can be seen in the results.

To confirm and refine this outcome, we recorded the angularly resolved scattering of our sample at some specific infrared wavelengths using a smaller angular step (1°). Figures 7 and 8 show the results of such measurements, respectively, at 1064 nm and 1490 nm.

Again, the concordance between theory and experiment is extremely satisfactory, especially with regard to the amplitude and location of the scattering resonance peaks appearing in the transmitted half-space.

The results reported in this Letter demonstrate how this spectro-scatterometer, whose features are, to our knowledge, unique on a global level, allows us to characterize with great accuracy either the spectral dependence of the transmittance (or reflectance) of a complex thin-film filter or that of its ARS. This upgraded instrument, SALSA 4, is now incorporated within the DIFFUSIF metrological platform [24] at Institut Fresnel.

Further work will be devoted to the implementation of wide spectral range polarizers on this setup to access SS and PP components of scattered light.

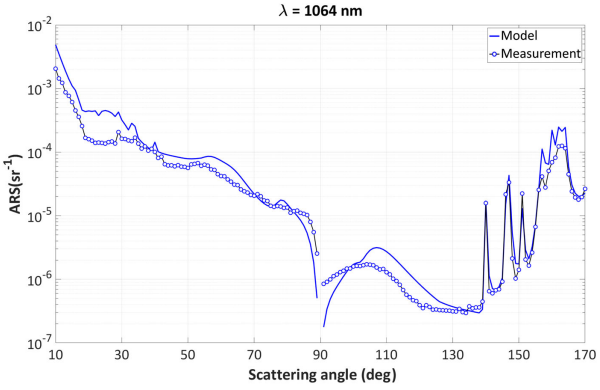


**Fig. 7.** Comparison between high angular resolution measurement of test filter ARS at 1064 nm and model prediction at the same wavelength.

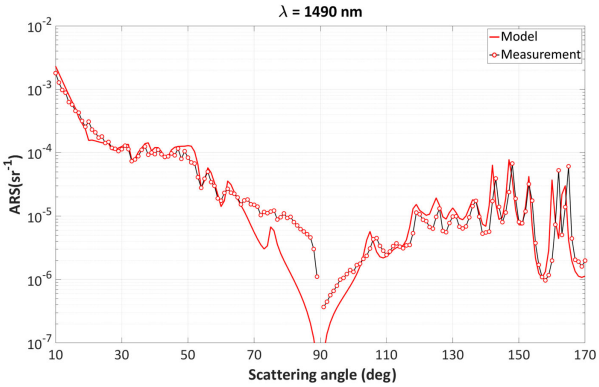


**Fig. 8.** Comparison between high angular resolution measurement of test filter ARS at 1490 nm and model prediction at the same wavelength.

**Funding.** Centre National d'Etudes Spatiales; CILAS Ariane Group.

**Disclosures.** The authors declare no conflicts of interest.

## REFERENCES

1. A. Johansen, A. Czajkowski, M. Scobey, P. Egerton, and R. Fortenberry, Alluxa white paper, 2017, https://www.alluxa.com/learning-center/white-papers/thin-film-interference-filters-for-lidar/.
2. Viavi Solutions White Paper, 2017, https://www.viavisolutions.com/en-us/literature/optical-filters-lidar-systems-white-paper-en.pdf.
3. J. W. Lichtman and J. A. Conchello, Nat. Methods **2**, 910 (2005).
4. M. K. Tilsch, R. B. Sargent, and C. A. Hulse, *Wavelength Filters in Fibre Optics* (Springer, 2006).
5. R. Le Goff, H. Krol, M. Lequime, B. Badoil, G. Montay, and K. Gasc, "Multispectral filters assemblies for earth remote sensing imagers," in *International Conference on Space Optics (ICSO)*, Tenerife (2014).
6. F. Lemarquis, T. Begou, A. Moreau, and J. Lumeau, CEAS Space J. **11**, 567 (2019).
7. D. Cheever, F. Cady, K. A. Klicker, and J. C. Stover, Proc. SPIE **818**, 13 (1987).
8. C. Amra, D. Torricini, and P. Roche, Appl. Opt. **32**, 5462 (1993).
9. T. A. Germer and C. C. Asmail, Rev. Sci. Instru. **70**, 3688 (1999).
10. A. von Finck, T. Herffurth, S. Schröder, A. Duparré, and S. Sinzinger, Appl. Opt. **53**, A259 (2014).
11. A. von Finck, T. Herffurth, A. Duparré, S. Schröder, M. Lequime, M. Zerrad, S. Liukaityte, C. Amra, S. Achour, M. Chalony, Q. Kuperman, Y. Cornil, A. Bialek, T. Goodman, C. Greenwell, B. Gur, S. Brinkers, G. Otter, A. Vosteen, J. Stover, R. Vink, A. Deep, and D. Doyle, Appl. Opt. **58**, 6638 (2019).
12. M. Lequime, S. Liukaityte, M. Zerrad, and C. Amra, Opt. Express **23**, 26863 (2015).
13. M. Lequime, M. Zerrad, and C. Amra, Opt. Express **26**, 34236 (2018).
14. NKT Photonics, https://www.nktphotonics.com/.
15. Photon Etc., http://www.photonetc.com/en/home2019.html.
16. FEMTO, https://www.femto.de/en/.
17. IRIDIAN Spectral Technologies, https://www.iridian.ca/.
18. ANDOR, https://andor.oxinst.com/?gclid=EAIaIQobChMIz6KQ8_G16AIVAVPTCh2D5wKJEAAYASAAEgKWivD_BwE.
19. M. Zerrad, S. Liukaityte, M. Lequime, and C. Amra, Appl. Opt. **55**, 9680 (2016).
20. M. Zerrad, M. Lequime, S. Liukaityte, and C. Amra, CEAS Space J. **9**, 473 (2017).
21. Labsphere, https://www.labsphere.com/.
22. P. B. Johnson and R. W. Christy, Phys. Rev. B **6**, 4370 (1972).
23. C. Amra, M. Lequime, and M. Zerrad, *Electromagnetic Optics in Thin-Film Coatings* (Cambridge University, 2020).
24. DIFFUSIF, https://www.fresnel.fr/diffusif.